AIAA 96-0062

EXPERIMENTS ON AIRFOILS AT LOW REYNOLDS NUMBERS

Michael S. Selig, James J. Guglielmo,
Andy P. Broeren and Philippe Giguère

University of Illinois at Urbana-Champaign
Urbana, IL

34th Aerospace Sciences Meeting & Exhibit

January 15-18, 1996 / Reno, NV

EXPERIMENTS ON AIRFOILS AT LOW REYNOLDS NUMBERS

Michael S. Selig,* James J. Guglielmo,† Andy P. Broeren‡ and Philippe Giguère†
Department of Aeronautical and Astronautical Engineering
University of Illinois at Urbana-Champaign
Urbana, Illinois 61801

Abstract

Lift and drag measurements were taken on 34 airfoils at low Reynolds numbers in an attempt to develop a consistent database for use in design studies that require accurate low Reynolds number airfoil data. From these data emerged several interesting results related to the behavior of the laminar separation bubbles and their effect on the lift characteristics. A plateau in the lift curve of symmetrical airfoils in the vicinity of an angle of attack of 0 deg was found to be common in the Reynolds number range of 40,000 to 100,000. Through the use of zig-zag type boundary-layer trips, this nonlinearity can be reduced owing to a reduction in the size of the laminar separation bubbles. The influence of laminar separation bubbles was also found to dominate the performance of several high-lift airfoils in the Reynolds number range of 80,000 to 150,000. In particular, hysteresis loops in the lift curve were present, and these are related to the size of the laminar separation bubble as deduced from drag data. The data reveals that some airfoils exhibit both counterclockwise and clockwise hysteresis loops for a given Reynolds number. Moreover, depending on the airfoil, either type of loop can occur first.

Introduction

A wide variety of small unmanned aerial vehicles (UAVs)[1] operate in the low Reynolds number regime in which the airfoil aerodynamics play a key role in aircraft performance and handling. In this regime, natural boundary-layer transition takes place through a laminar separation bubble that forms as the laminar boundary layer first separates, then becomes unstable, makes a transition to turbulent flow and reattaches to the airfoil to form a laminar separation bubble.[2,3] This bubble often results in a notable airfoil-performance degradation that is characterized by undesirable high drag, nonlinearities in the lift-curve characteristics and sometimes static hysteresis in the section lift, drag and moment data.[4,5]

In an effort to understand the flow phenomena at low Reynolds numbers, there have been numerous theoretical and experimental investigations that have resulted in three conferences[6–8] and a special AGARD publication.[9] Because of the difficulty in modeling the laminar separation bubble, computational efforts, while vital for use in design, have not been entirely reliable in predicting these complex flows. Nonetheless, considerable progress has been made in recent years.[10–16]

Despite the high level of interest in this area, few systematic experiments have been performed to document the performance of a wide selection of airfoils for use in conceptual and detailed design studies. This has been particularly problematic because comparisons of data between different wind tunnels facilities regularly show discrepencies owing to the documented difficulties in measuring low Reynolds number airfoil performance. Thus, the mixture of different data sets is not ideally suited for the purposes of examining performance trade-offs involving different airfoils.

A key objective of the present research was to produce a large and consistent low Reynolds number airfoil performance database for use in the design of small UAVs. Specifically, the experiments[17] involved measuring the lift and drag characteristics of many airfoils over the nominal Reynolds number range of 60,000 to 300,000. The collection of airfoils tested is depicted in Fig. 1.

The more limited objective of this paper is to highlight and explain two interesting features observed in the lift characteristics of some of the airfoil tested. In particular, this paper presents and discusses (1) the nonlinear lift characteristics of two symmetrical airfoils (NACA 0009 and SD8020) as well as improvements made through the use of boundary-layer trips, and (2) the hysteresis in the lift characteristics of six high-lift airfoils (FX 63-137, S1210, modified FX 74-CL5-140, CH 10-48-13, M06-13-128 and S1223). As will be described, both features, the nonlinearity and the hysteresis of the lift curves, can be linked to the behavior of the laminar separation bubbles.

*Assistant Professor. Member AIAA.

†Graduate Research Assistant. Student Member AIAA.

‡Graduate Research Assistant.

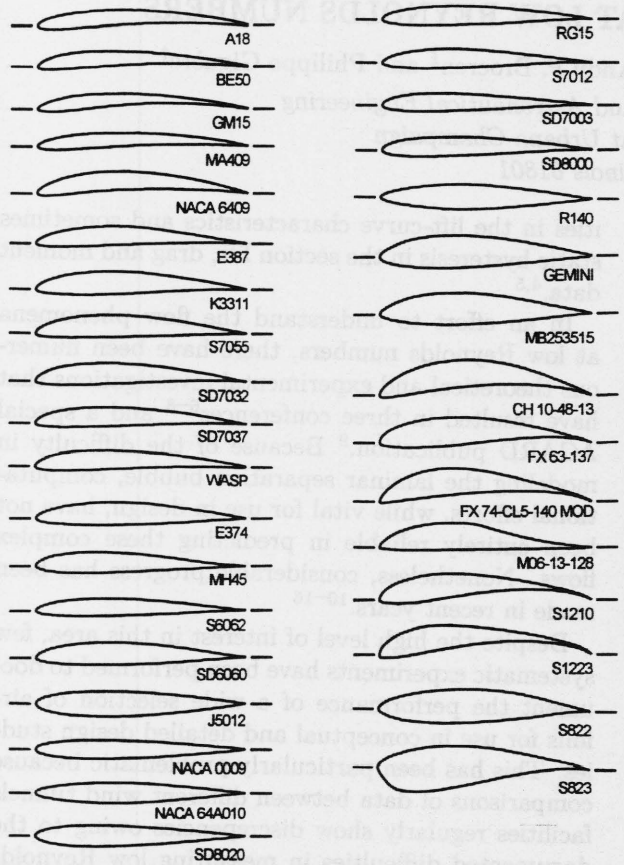

Fig. 1 The 34 airfoils tested.

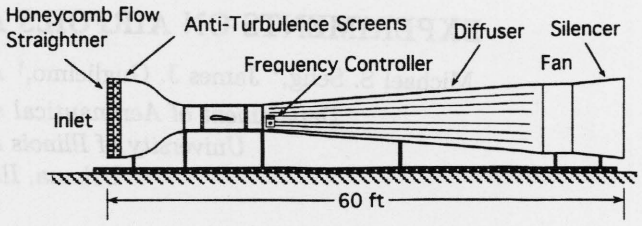

Fig. 2 UIUC low-speed subsonic wind tunnel.

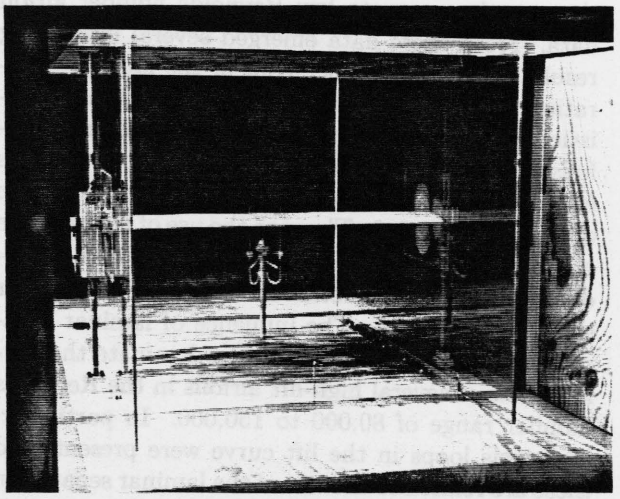

Fig. 3 Photograph of the wind-tunnel test section.

Experimental Apparatus and Techniques

The discussion of the experimental apparatus and measurement techniques will be brief since more details can be found in Ref. 19.

Wind Tunnel

All experiments were performed in the University of Illinois at Urbana-Champaign (UIUC) open-return subsonic wind tunnel (Fig. 2). The dimensions of the rectangular test-section are approximately 2.8 × 4 ft in cross-section and 8 ft long. In order to ensure good test-section flow quality, the tunnel settling chamber contains a 4 in thick sheet of honeycomb and four anti-turbulence screens, resulting in a test section turbulence level of less than 0.1% over the 3–55 mph speed range required for these tests.

Airfoil Models

All models had a 12 in chord and 33 5/8 in span. To isolate the ends of the model from the tunnel side-wall boundary layers and the support hardware, the models were mounted horizontally between two 3/8 in thick, 6 ft long Plexiglas splitter plates (see Fig. 3). The gap between the model and Plexiglas was nominally 0.05 in.

To assess the accuracy of the models, the airfoil section at the mid-span of each model was digitized using a Brown & Sharpe coordinate measuring machine. These measured coordinates were compared with the true coordinates using a least squares approach. For the eight airfoils discussed in this paper, model accuracies of better than 0.010 in (averaged over the 12 in chord) were typical.

Data Acquisition, Reduction and Validation

The data acquisition process was completely automated, including setting and maintaining a constant airfoil chord Reynolds number. The lift was measured with a servo feedback-controlled force balance, and drag was obtained from the momentum method. To ensure that the wake had relaxed to tunnel static pressure, the wake measurements were performed 14.8 in (approximately 1.25 chord lengths) downstream of the trailing edge of the airfoil. To obtain an accurate value for the drag coefficient, the wake profile was measured at four spanwise stations spaced 4 in apart over the center 12 in of the airfoil.

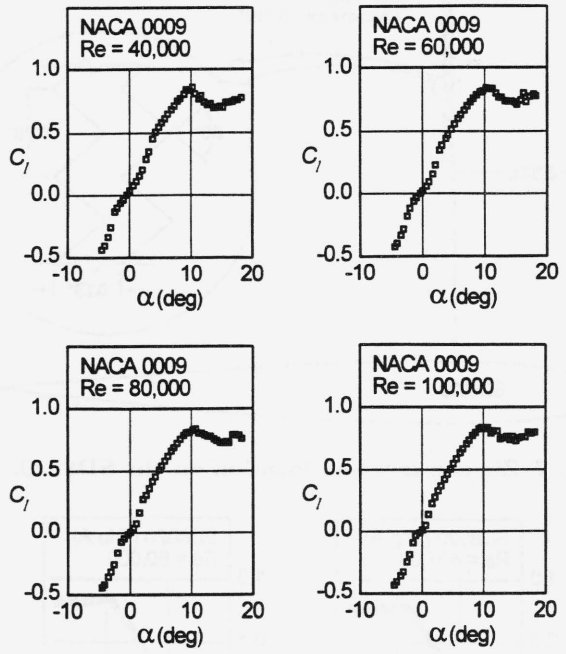

Fig. 4 Lift characteristics for the NACA 0009.

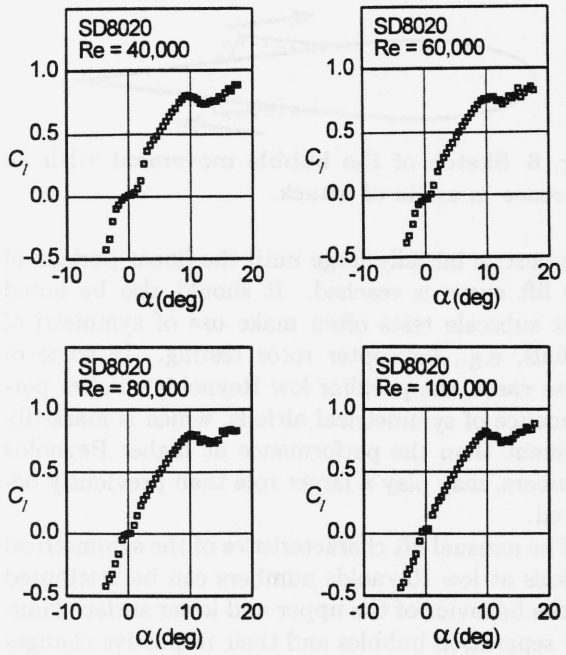

Fig. 5 Lift characteristics for the SD8020.

The resulting four drag coefficients were then averaged to obtain the drag at a given angle of attack.

The lift, drag and angle of attack measurements were corrected for solid blockage, wake blockage and streamline curvature effects.[20] The freestream velocity was not only corrected for solid and wake blockage effects but also for a "circulation effect" that was particular to the setup shown in Fig. 3. As previously mentioned, the models were mounted between splitter plates inserted in the test section. The use of splitter plates required that the freestream velocity be measured between them due a spillage effect (air flowing between the splitter plates and the tunnel side walls). Since the freestream pitot-static probe was located fairly close to the model, the measurements were corrected for airfoil circulation effects. The details of this correction can be found in Ref. 21.

The overall uncertainty is estimated to be 1.5% for the lift and 4.5% for the drag (3% of which is due to the spanwise variation in the drag). Comparison of the data for the E387 baseline model[17] showed good agreement with data taken at NASA Langley,[22] Delft,[23] and Stuttgart.[24] Discrepancies that did exist can be attributed largely to the slight decamber of the model.

Results and Discussion

Lift Characteristics of Symmetrical Airfoils

Lift characteristics for the NACA 0009 airfoil at Reynolds numbers of 40,000, 60,000, 80,000 and 100,000 are shown in Fig. 4. As seen, the lift characteristics are not typical of those found for higher Reynolds number airfoil flows in which the lift curve is nearly linear with a slope of 2π. For each Reynolds number, the lift curve slope is initially less than 2π and then greater before it resumes the more typical linear charactistic until stall.

The peculiar nonlinear features of the lift curve around 0 deg angle of attack are not unique to the NACA 0009 airfoil. For example, Figure 5 shows the lift characteristics of the symmetrical, 10%-thick SD8020 airfoil[25] over the same Reynolds number range. Moreover, for the symmetrical NACA 66_3-018 airfoil, Mueller & Batill[26] found a similar result at a Reynolds number of 130,000. For small positive angles of attack the C_l was not only reduced but in fact negative (e.g, for $\alpha \approx 1$ deg, $C_l \approx -0.1$). More recently, Sato & Sunada[27] tested a 28.57% thick symmetrical NACA airfoil at $Re = 33,000$ and found that the airfoil developed negligiblelift throughout its normal operating range.

The unusual lift characteristics of symmetrical airfoils at low Reynolds numbers is not desirable. Low Reynolds number UAVs can have unusual longitudinal handling characteristics when full-flying symmetrical stabilators are used. The shallow lift-curve slope about 0 deg angle of attack can make an aircraft (when trimmed with nearly zero load on the tail) feel sluggish as a result of the "deadband" in the lift curve. Moreover, as in the case of the NACA 66_3-018, there may even be a control reversal over a small ± 2 deg range. Outside of this range, however, the

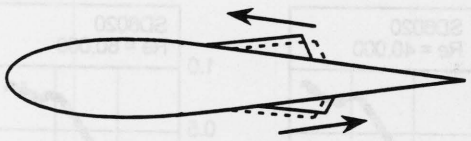

Fig. 6 Sketch of the bubble movement with an increase in angle of attack.

response is initially large until the linear portion of the lift curve is reached. It should also be noted that subscale tests often make use of symmetrical airfoils, e.g., helicopter rotor testing. In some of these cases, the peculiar low Reynolds number performance of symmetrical airfoils, which is markedly different than the performance at higher Reynolds numbers, may play a larger role than previously believed.

The unusual lift characteristics of the symmetrical airfoils at low Reynolds numbers can be attributed to the behavior of the upper and lower surface laminar separation bubbles and their respective changes in size with angle of attack. As the angle of attack is increased, the pressure gradient on the upper surface steepens, and the upper surface bubble grows larger. This growth in the size of the bubble (sketch in Fig. 6) is supported by flow visualization studies.[25,26] The larger bubble increases the displacement thickness, which effectively introduces negative camber. On the lower surface, the opposite occurs. The pressure gradient becomes more favorable, the bubble shrinks in size, and the displacement thickess decreases, which in turn introduces more negative camber. In effect the negative camber adds reflex to the otherwise non-cambered airfoil. Consequently, the lift is reduced relative to what might be expected when laminar separation bubble effects are ignored. This loss in lift accounts for the initial deadband in the vicinity of 0 deg angle of attack.

The lift reversal of NACA 66_3-018 observed by Mueller & and Batill[26] can be explained similarly by the effects of laminar separation bubbles. The NACA 66_3-018 airfoil was designed as a laminar flow airfoil and as such has favorable pressure gradients followed by a relatively steep pressure recovery (as compared with that of the NACA 0009). At low Reynolds numbers, laminar separation on the airfoil takes place far aft in the pressure recovery region.[26] As a result, the bubbles are rather large and their effects are amplified accordingly. When the angle of attack is increased to 1 deg, the size of the bubble on the upper surface increases, while on the lower surface it decreases as previously discussed. The bubbles are so much larger, however, that negative lift is produced.

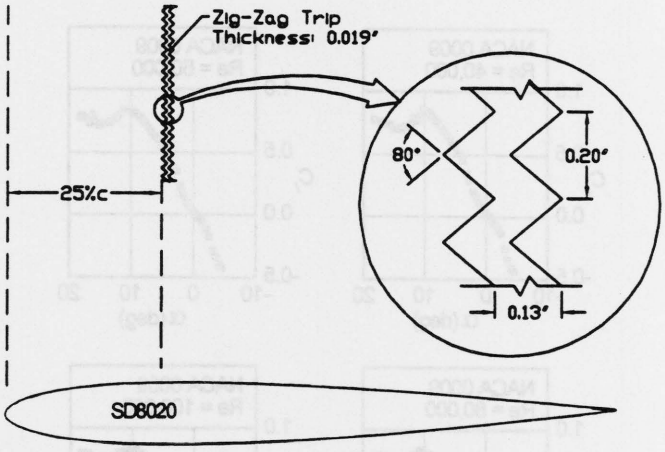

Fig. 7 Zig-zag trip and location on the SD8020.

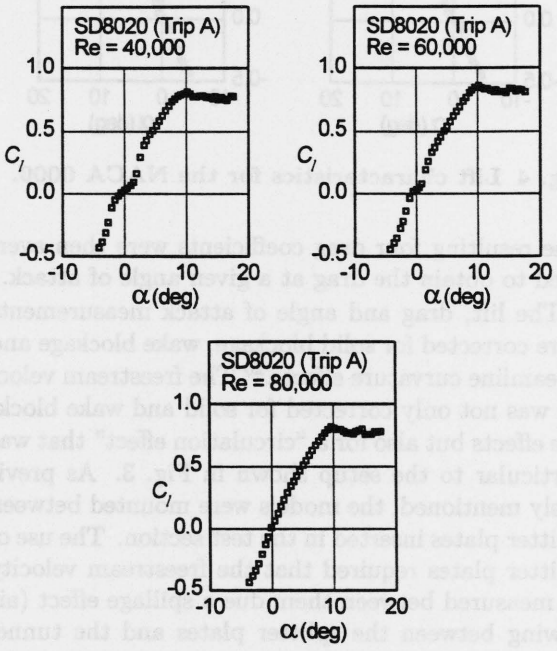

Fig. 8 Lift characteristics for the SD8020 with zig-zag trips (1 layer — Trip A).

Beyond the deadband (or reversal region), the lift-curve slope steepens and resumes the characteristic features of lift curves at higher Reynolds numbers. The steepening of the lift curve is caused by a reduction in the size of the bubble as it moves toward the leading edge. This is likewise accompanied by a reduction in the drag as well.

Since the poor lift characteristics are caused by laminar separation bubbles, boundary layer trips can be expected to improve the performance. This approach was taken in an attempt to improve the lift characteristics of the SD8020. First, one layer of zig-zag trip tape (Trip A) with a thickness of 0.019 in was placed on both the upper and lower

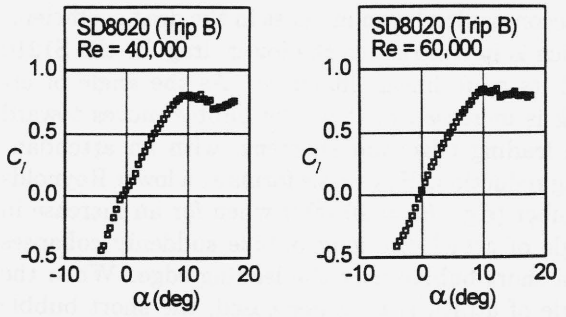

Fig. 9 Lift characteristics for the SD8020 with zig-zag trips (2 layers — Trip B).

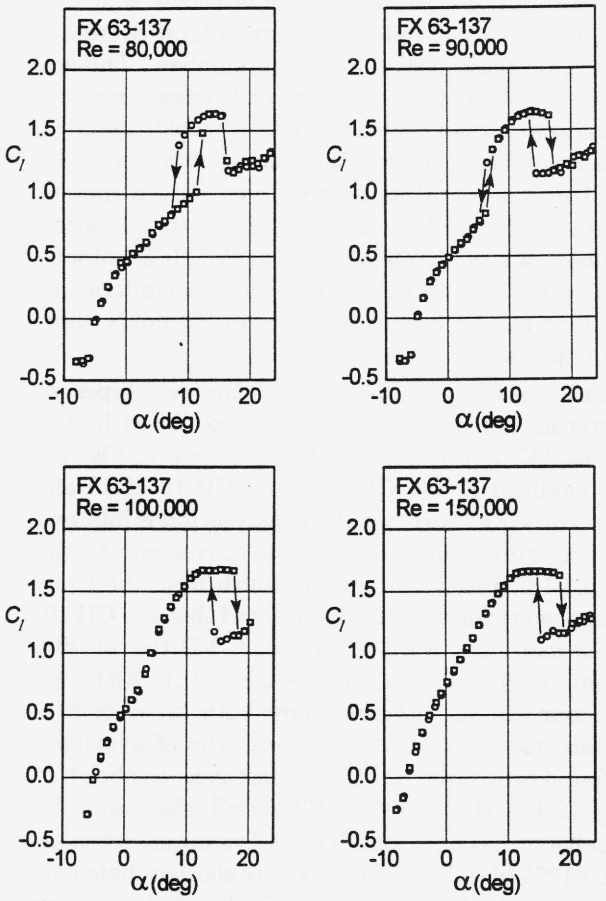

Fig. 10 Lift characteristics for the FX 63-137.

surfaces at 25% chord (see Fig. 7). As seen in Fig. 8, the nonlinearity (deadband) is reduced up to $Re = 80,000$, after which it is completely eliminated. Second, two layers of the zig-zag trip (Trip B) were used, and the effects of the bubbles were eliminated between $Re = 40,000$ and 60,000 (see Fig. 9). At $Re = 40,000$, however, the lift characteristics are greatly improved over the baseline case without trips.

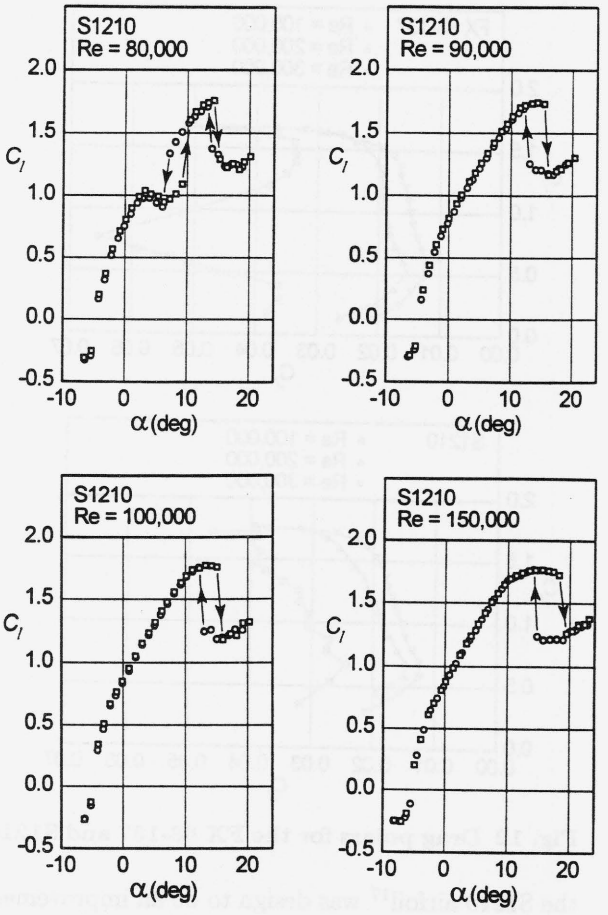

Fig. 11 Lift characteristics for the S1210.

It should also be mentioned that behavior of the bubbles as described can also be deduced from drag data as well. For both the NACA 0009 and SD8020 at a Reynolds number of 60,000 as well as several other similar symmetrical airfoils,[17,25] the drag increased in going from an angle of attack of 0 deg to ±1 deg. This trend is consistent with a substantial growth in the size of the suction-side bubble. Moreover, when boundary-layer trips were used, the increase in the drag about 0 deg angle of attack was eliminated and the overall drag was reduced.

Airfoil Static Lift Hysteresis

For some airfoils at low Reynolds numbers, the performance data depends on whether the given test condition was obtained through an increase or decrease in angle of attack or Reynolds number. For example, hysteresis is seen in the lift characteristics of both the FX 63-137 and S1210 shown in Figs. 10 and 11, respectively. (In the figures, increasing and decreasing angles of attack are denoted by square and circle symbols, respectively.) The FX 63-137 airfoil is among the most desirable airfoils for high-lift, low Reynolds number UAV applications,[28,29] while

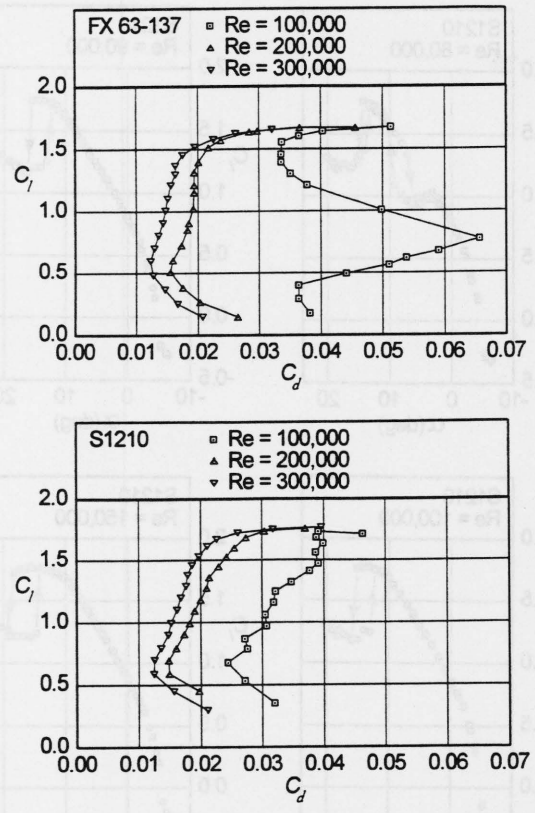

Fig. 12 Drag polars for the FX 63-137 and S1210.

the S1210 airfoil[17] was design to be an improvement over the FX 63-137.

These two airfoils exhibit clockwise and counterclockwise hysteresis loops, which are representative of the two general types of lift hysteresis observed at low Reynolds numbers. Although these two types of hysteresis have been given names in the literature,[30,31] they will be called here for the sake of discussion long-bubble (counterclockwise) and short-bubble (clockwise) hysteresis. As the names imply, the hysteresis loops are related to the type of laminar separation bubbles.

Short-bubble hysteresis, which occurs at $C_{l,max}$ for the FX 63-137, is caused by a short bubble that remains attached until stall. As the angle of attack is then decreased, the bubble does not reattach until a lower angle of attack is reached.

Long-bubble hysteresis for the FX 63-137 occurs in the mid-lift range (see $Re = 80,000$ and 90,000 cases). Prior to its formation, a nonlinearity appears in the lift curve in the mid-lift range (see $Re = 100,000$ case). Interestingly, this precursor to long-bubble hysteresis is closely associated with the deadband of symmetrical airfoils previously discussed. For the FX 63-137 at $Re = 100,000$, the upper-surface bubble grows larger with an increase in angle of attack. As shown in Fig. 12, this process is accompanied by an increase in the drag coefficient, which is in contrast to the lower drag for the S1210 and its more linear lift curve. As the angle of attack is increased further, the bubble moves toward the leading edge and shortens, with an attendant drag reduction. Hysteresis forms at a lower Reynolds number (e.g., $Re = 90,000$) when for an increase in angle of attack the long bubble suddenly collapses to a short bubble near the leading edge. When the angle of attack is then decreased, the short bubble remains attached until a lower angle of attack, at which condition it bursts into a long bubble.

An interesting feature can be found in the data. For both airfoils, the stall angle of attack that terminates the short-bubble hysteresis loop decreases with a decrease in the Reynolds number. The angle of attack at which the flow reattaches, however, remains essentially constant with Reynolds number. The Reynolds number dependence is consistent with the behavior of full-separated flows (which dictate the reattachment boundary) and laminar separation bubbles (which dictate the stall angle). It is not surprising to find, therefore, that both boundaries of the long-bubble hysteresis loop are Reynolds number dependent.

The possible combinations of the two types of hysteresis are not limited to those exhibited by the FX 63-137 and S1210 airfoils. As shown in Fig. 13, the modified FX 74-CL5-140 and CH 10-48-13 airfoils first have short-bubble hysteresis loops followed by long-bubble hysteresis loops, in contrast to the FX 63-137 and S1210 airfoils which have the loops in opposite order. It should be noted that the CH 10-48-13 made use of a 0.023 in thick 2-D trip at 40% chord on the upper surface (see Fig. 14). Although the four airfoils discussed have both types of hysteresis, most commonly only one type of hysteresis is found on a given airfoil. For instance, as shown in Fig. 13 the Miley M06-13-128 airfoil, also tested by Mueller,[31] has only long-bubble hysteresis; whereas, the S1223 high-lift airfoil has only short-bubble hysteresis much like the Lissaman 7769 airfoil tested by Mueller.[31]

Conclusions

A recent series of tests on low Reynolds number airfoils have lead to a better understanding of the peculiar features found in the lift characteristics of airfoils at low Reynolds numbers. For symmetrical airfoils, the nonlinear features in the lift curve about 0 deg angle of attack are more common than previously believed. As compared with past research, these problems are compounded by an increase in the airfoil thickness and the length of the favorable

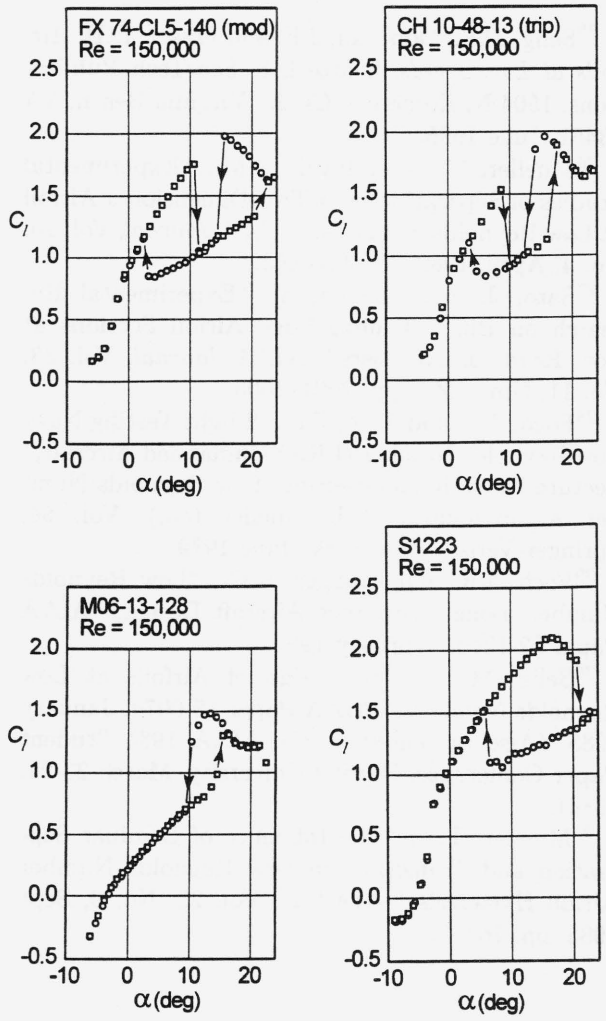

Fig. 13 Lift characteristics for the modified FX 74-CL5-140, CH 10-48-13, M06-13-128 and S1223.

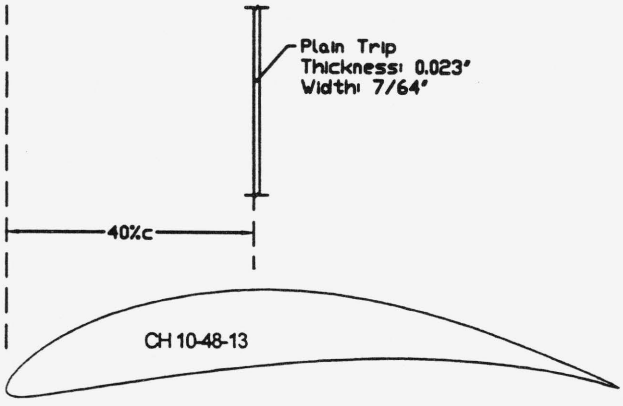

Fig. 14 Plain trip used on the CH 10-48-13.

pressure gradient, both of which tend to steepen the pressure recovery. The steep pressure recovery promotes a long laminar separation bubble, which ultimately drives the undesirable lift characteristics of symmetrical airfoils about 0 deg angle of attack. Boundary-layer trips appropriately positioned and sized can mitigate these adverse effects for Reynolds numbers as low as 40,000 for airfoils that are approximately 10% thick. Thus, it is recommended that boundary-layer trips be used on symmetrical airfoils at low Reynolds numbers, especially when operated near 0 deg angle of attack.

Tests on a six high-lift airfoils have revealed that some airfoils exhibit two types of hysteresis, named here long-bubble and short-bubble hysteresis after the type of bubble most associated with the hysteresis. In some cases, long-bubble hysteresis is followed by short-bubble hysteresis and vice versa. More commonly, only short-bubble or long-bubble hysteresis is present, while sometimes no hysteresis exists.

Acknowledgments

This research was supported through the private donations to the University of Illinois. The authors wish to thank Mark Allen, Yvan Tinel, Ray Olsen, Ron Wagner, Mark Nankivil and Chuck Hollinger for their skillful efforts in the fabrication of the wind tunnel models. Cameron Ninham also made significant contributions to this work.

References

[1]Munson, K., *World Unmanned Aircraft*, Jane's Publishing, Inc., 1988.

[2]Gaster, M., "The Structure and Behavior of Laminar Separation Bubbles," NPL Aero Report 1181, ARC 28,226, 1966.

[3]Tani, I., "Low-Speed Flows Involving Bubble Separation," *Progress in Aeronautical Sciences*, Vol. 5, MacMillan Co., 1974.

[4]Carmichael, B.H., "Low Reynolds Number Airfoil Survey Volume I," NASA CR 165803, Nov. 1981.

[5]Lissaman, P.B.S., "Low Reynolds Number Airfoils," *Annual Review of Fluid Mechanics*, Vol. 15, pp.223–239, 1983.

[6]*Proceedings of the Conference on Low Reynolds Number Airfoil Aerodynamics*, UNDAS-CP-77B123, University of Notre Dame, Notre Dame, Indiana, June 1985.

[7]*Proceedings of the Aerodynamics at Low Reynolds Numbers* $10^4 < Re < 10^6$ *International Conference*, London, October 1986.

[8]*Lecture Notes in Engineering: Low Reynolds Number Aerodynamics*, T.J. Mueller (ed.), Vol. 54, Springer-Verlag, New York, June 1989.

[9]Mueller, T.J., *Low Reynolds Number Vehicles*, AGARDograph No. 288, Feb. 1985.

[10]Eppler, R. and Somers, D.M., "A Computer Program for the Design and Analysis of Low-Speed

Airfoils," NASA TM 80210, August 1980.

[11]Eppler, R., *Airfoil Design and Data*, Springer-Verlag, New York, 1990.

[12]Drela, M. and Giles, M.B., "ISES: A Two-Dimensional Viscous Aerodynamic Design and Analysis Code," AIAA Paper 87-0424, January 1987.

[13]Drela, M. and Giles, M.B., "Two-Dimensional Transonic Aerodynamic Design Method," *AIAA Journal*, Vol. 25, No. 9, September 1987, pp. 1199–1206.

[14]Drela, M., "XFOIL: An Analysis and Design System for Low Reynolds Number Airfoils," in *Lecture Notes in Engineering: Low Reynolds Number Aerodynamics*, T.J. Mueller (ed.), Vol. 54, Springer-Verlag, New York, June 1989.

[15]Dini, P. and Maughmer, M.D., "Locally Interactive Laminar Separation Bubble Model," *J. of Aircraft*, Vol. 31, No. 4, July-Aug. 1994, pp. 802–810.

[16]Shum, Y.K. and Marsden, D.J., "Separation Bubble Model for Low Reynolds Number Airfoil Applications," *J. of Aircraft*, Vol. 31, No. 4, July-Aug. 1994, pp. 761–766.

[17]Selig, M.S., Guglielmo, J.J., Broeren, A.P. and Giguère, P., *Summary of Low-Speed Airfoil Data*, Vol. 1, SoarTech Publications, 1504 N. Horseshoe Circle, Virginia Beach, VA 23451, June 1995.

[18]Guglielmo, J.J. and Selig, M.S., "Large Spanwise Variations in Profile Drag for Airfoils at Low Reynolds Numbers," AIAA Paper 95-1783, June 1995.

[19]Guglielmo, J.J., "Spanwise Variations in Profile Drag for Airfoils at Low Reynolds Numbers," Master's Thesis, University of Illinois at Urbana-Champaign, Department of Aeronautical and Astronautical Engineering, 1996.

[20]Rae, W.H., Jr. and Pope, A., *Low-Speed Wind Tunnel Testing*, John Wiley and Sons, New York, 1984.

[21]Giguère, P, "Two-Dimensional Wind Tunnel Boundary Layer Corrections for Low-Speed Testing in a Rectangular Test Section," University of Illinois, Report number to be assigned, 1995.

[22]McGhee, R.J., Jones, G.S., and Jouty, R., "Performance Characteristics from Wind-Tunnel Tests of a Low-Reynolds-Number Airfoil," AIAA Paper 88-0607, January 1988.

[23]Volkers, D. F., "Preliminary Results of Wind Tunnel Measurements on Some Airfoil Sections at Reynolds Numbers between 0.6×10^5 and 5.0×10^5," Memo M-276, Delft University of Technology, The Netherlands, 1977.

[24]Althaus, D., *Profilpolaren fur den Modellflug*, Necker-Verlag, Villingen-Sch-wenningen, FRG, 1980.

[25]Selig, M.S., Donovan, J.F. and Fraser, D.B, *Airfoils at Low Speeds*, Soartech 8, SoarTech Publications, 1504 N. Horseshoe Circle, Virginia Beach, VA 23451, June 1995.

[26]Mueller, T.J and Batill, S.M., "Experimental Studies of Separation on a Two-Dimensional Airfoil at Low Reynolds Numbers," *AIAA Journal*, Vol. 20, No. 4, April, 1982, pp. 457–463.

[27]Sato, J. and Sunada, Y, "Experimental Research on Blunt Trailing-Edge Airfoil Sections at Low Reynolds Numbers," *AIAA Journal*, Vol. 33, No. 11, Nov. 1995, pp. 2001–2005.

[28]Foch, J.R. and Toot, P.L., "Flight Testing Navy Low Reynolds Number (LRN) Unmanned Aircraft," Lecture Notes in Engineering: Low Reynolds Number Aerodynamics, T.J. Mueller (ed.), Vol. 54, Springer-Verlag, New York, June 1989.

[29]Foch, J.R. and Ailinger, K.G., "Low Reynolds Number, Long Endurance Aircraft Design," AIAA Paper 92-1263, February 1992.

[30]Selig, M.S., "The Design of Airfoils at Low Reynolds Numbers," AIAA Paper 85-0074, January 1985. (Also presented at the AIAA 1984 Student Paper Conference, Purdue University, March 23-24, 1984).

[31]Mueller, T.J., "The Influence of Laminar Separation and Transition on Low Reynolds Number Airfoil Hysteresis," *AIAA J.*, Vol. 22, No. 9, Sept 1985, pp. 763–770.